Research Article | Vol. 26, No. 14 | 9 Jul 2018 | OPTICS EXPRESS 17872
Optics EXPRESS

Ray-optical transformation optics with ideal thin lenses makes omnidirectional lenses

JOHANNES COURTIAL,[1,*] TOMÁŠ TYC,[2] JAKUB BĚLÍN,[1] STEPHEN OXBURGH,[1] GERGELY FERENCZI,[1] EUAN N. COWIE,[1] AND CHRIS D. WHITE[3]

[1] *School of Physics & Astronomy, College of Science & Engineering, University of Glasgow, Glasgow G12 8QQ, UK*
[2] *Institute of Theoretical Physics and Astrophysics, Masaryk University, Kotlarska 2, 61137 Brno, Czech Republic*
[3] *Centre for Research in String Theory, Queen Mary University of London, 327 Mile End Road, London E1 4NS, UK*
[*] *Johannes.Courtial@glasgow.ac.uk*

Abstract: We present the theory of ray-optical transformation optics (RTO) with ideal thin lenses and show that ideal-thin-lens RTO devices are omnidirectional lenses. Key to designing such devices are two theorems, the *loop-imaging theorem*, and the *edge-imaging theorem*, which ensure that the interior physical space is distorted in the same way for all viewing directions. We discuss the possibility of realising such devices using lens holograms or Fresnel lenses, as both are in principle capable of changing the directions of rays incident from a specific point *precisely* like an ideal thin lens, thereby enabling macroscopic and broad-band RTO devices that work for at least one viewing position. Even when restricted in this way, our work opens up new possibilities in ray optics. Our devices have the potential to form the basis of new microscope objectives, virtual-reality headsets, and medical spectacles.

1. Introduction

Transformation optics (TO) [1,2] is a relatively new, and highly active, research field. It uses the mathematics of differential geometry to design novel structures, capable of bending light in interesting ways. The theory is particularly attractive if arbitrary material properties are allowed, which can, with some limitations, be realised in the form of metamaterials. A much-publicised example device is the invisibility cloak, a metamaterial structure that steers incident light around a central volume, such that the outgoing light rays appear undeviated. Any object in the central region is thus rendered invisible, as is the cloak itself if other effects in the material (absorption, polarisation change, etc.) are neglected. This raised hopes of the imminent arrival of Harry-Potter-style invisibility cloaks; one decade on, however, very significant difficulties still need to be overcome before metamaterial structures that allow white-light, macroscopic cloaking [3] become feasible.

These deficiencies have motivated a number of alternative realisations of TO ideas. The resulting devices are significantly easier to realise, but work only for light rays, not waves. Examples of such ray-optical TO (RTO) devices include multidirectional prism structures [4], arrangements of lenses and mirrors [5], and even digital cloaks [5] based on the ideas of integral photography [6]. Particularly relevant to this study are the "Rochester cloak", a combination of four lenses that can hide objects placed in certain places when viewed from a small range of directions [7], and our own theoretical proposals for omnidirectional cloaks consisting of planar, microstructured *telescope windows* [8–10]. The latter can be understood as involving pixellated approximations of generalisations of ideal thin lenses called *glenses* [11], in which the object- and image-sided focal lengths are different. In the cloaks described in Refs [8,9], both

#329016 https://doi.org/10.1364/OE.26.017872
Journal © 2018 Received 20 Apr 2018; revised 20 Jun 2018; accepted 21 Jun 2018; published 26 Jun 2018

Optics EXPRESS

focal lengths of each glens are different (specifically differently infinite, as is the distance of the optical axis, meaning the glenses are homogeneous [12]). In the cloak described in [10], the focal lengths of several glenses are equal, which means that these glenses are simply ideal thin *lenses*. This motivated the question "Is it possible to design omnidirectional RTO devices purely from ideal thin lenses?"

Here we answer this question affirmatively by constructing an example of an (omnidirectional) RTO device comprising exclusively ideal thin lenses. Interestingly, this structure can be interpreted as an omnidirectional lens (as well as a novel type of cloak [13]). We derive two theorems that can be used to determine if a given ideal-thin-lens structure is an RTO device. Ideal thin lenses do not currently exist in reality, and therefore ideal-thin-lens RTO devices cannot currently be realised. However, it is possible to realise approximations to such devices that accept compromises. We discuss one such approximation, which restricts the resulting devices to work perfectly (in principle) for a single arbitrary, fixed, viewing position. We show that, even with this severe restriction, there are a number of potential applications of such devices.

2. Imaging in RTO devices

When viewed from the outside, the inside of a TO device appears distorted. The distortion is the same for each outside viewing position — there is a unique mapping from any point inside a TO device to a corresponding point as seen by an outside observer. This enables the definition of two spaces: the actual structure is said to be in physical space, the apparent structure as seen from the outside is said to be in virtual space, and the "T" in (R)TO refers to the coordinate transformation that maps the two spaces. We use the existence of this coordinate transformation as the definition of a TO device; if the coordinate transformation maps only rays, but not waves, it defines an RTO device.

To describe RTO in terms of imaging, consider light rays that intersect at a given point A inside an RTO device, in physical space, and which may be contrasted with the point A′ where the straight-line continuations of the outside segments intersect (Fig. 1(a)), which is the corresponding point in virtual space. If a small object is placed at a physical-space position A, it appears to be located at the corresponding virtual-space position A′ when seen from outside the RTO device.

That the distortion between physical space and virtual space is the same for each outside viewing position implies the existence of a unique mapping from physical space to virtual space. (Note that this mapping can be many-to-one, as several physical-space positions can map to the same virtual-space position. An example can be seen in Fig. 1(a), where the positions of ray intersections in cells 1 (labelled A) and 2 (not labelled) are two physical-space positions that correspond to the same virtual-space position, A′.) As every ideal thin lens forms a unique image of every point, any physical-space position is mapped to a unique virtual-space position when seen through any particular combination of such lenses. But in the ideal-thin-lens cloak, the same physical-space positions can be seen from outside the cloak through *different* combinations of lenses, and it is by no means obvious that every one of these combinations images every point to the same position. For example, Fig. 1(a) is drawn such that A is imaged to A′ irrespective of whether the relevant light rays travel from A to the outside through lens L_{01} or through the combination of lenses L_{12}, L_{24}, and L_{04}. In an RTO device, this must hold for all lens combinations encountered along *any* path to the outside, and below we will construct an ideal-thin-lens structure in which this is indeed the case. We show this using two theorems called the *loop imaging theorem* and the *edge-imaging theorem* which we derive below, and which we also use to calculate the focal lengths of the lenses.

Consider the ideal-thin-lens structure shown in Fig. 1(a). The lenses divide the space inside the structure into polyhedral cells numbered 1 to 5 (1 to N in the general case of a device with N interior cells); the exterior is cell 0. The lens L_{ij} at the boundary of cells i and j performs optical

Optics EXPRESS

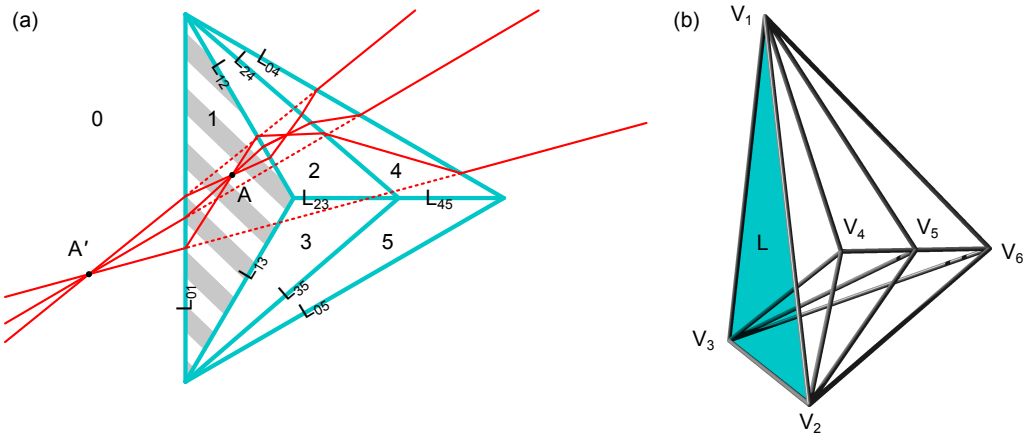

Fig. 1. Simple ideal-thin-lens structure, S, that forms an ideal-thin-lens RTO device. (a) A number of light-ray trajectories (red solid lines) through S, drawn for clarity in two dimensions (2D), are shown. The light-ray trajectories intersect at a physical-space position A inside S; the straight-line continuations (dotted red lines) of the outside segments of those same light-ray trajectories intersect in the virtual-space position A′. The ideal thin lenses (cyan lines) divide physical space inside S into cells numbered 1, 2, 3, etc.; cell 0 is the outside of the device. (b) In the full 3D structure, the respective roles of polygon vertices and edges in the 2D structure are played by polyhedron edges and faces. Each grey cylinder marks the common edge of two or more ideal thin lenses with a triangular clear aperture; wherever three of the cylinders form a triangle, this triangle forms the clear aperture of an ideal thin lens, of which there are 16 in total. For example, the shaded triangle with vertices V_1, V_2, and V_3 forms the clear aperture of a lens labelled L, which corresponds to lens L_{01} in (a). V_1 to V_3 form an equilateral triangle; V_4 to V_6 lie on a straight line perpendicular to this triangle and intersecting it at its center. The principal points of all lenses in S lie on this straight line. Note that the principal point coincides with the center of the clear aperture only in the case of lens L.

imaging between cells i and j; we denote the mapping from cell i to cell j as c_{ji}. Note that the order of the lens indices does not matter, but that of the indices of the mapping does. As the inside of each cell is empty, light rays therein travel in straight lines. Consequently, points that lie on the same straight line must be mapped to points that lie on another straight line, hence the mappings c_{ij} between neigbouring cells are collineations [14].

To find the virtual-space image A′ of a point A in some cell (say cell i) formed by rays that passed successively through lenses $L_{ij}, L_{jk}, \ldots, L_{m0}$ (the last lens being at the outer surface of the lens structure), we simply combine the corresponding mappings, and so

$$\mathrm{A}' = c_{0m} \cdots c_{kj} c_{ji} \mathrm{A}. \tag{1}$$

By our definition of an RTO device, the lens structure will be an RTO device if and only if the position A′ is independent of the lens combination by which light can reach the exterior of the device (cell 0) from cell i. If this is the case, then we can define a unique mapping C_i from that cell to the exterior of the device, cell 0, according to $C_i = c_{0m} \cdots c_{kj} c_{ji}$, and as cell i is an arbitrary cell, we can do this for any cell. The mapping C_i determines where points in that cell appear when observed from the outside; it is therefore the mapping of cell i of physical space to virtual space.

It should be clear that the mapping C_0 is the identity map: any physical space position outside the device appears at that same (virtual-space) position, irrespective of whether it is seen through

Optics EXPRESS

the RTO device or not. This implies that, in the absence of absorption effects etc., an RTO device is *invisible*.

The lens structure will be an RTO device if and only if the combined mapping $c_{0m} \cdots c_{kj} c_{ji}$ does not depend on the path $i \to j \to k \to \cdots \to m \to 0$ by which we reach cell 0 from cell i. In other words,

$$c_{0m} \cdots c_{kj} c_{ji} = c_{0m'} \cdots c_{k'j'} c_{j'i} \tag{2}$$

must hold, where $i \to j' \to k' \to \cdots \to m' \to 0$ is another path from cell i to cell 0. Thanks to the property $c_{ij} = c_{ji}^{-1}$ (the mapping from cell j to cell i is the inverse of the mapping from cell i to cell j), we can rewrite this equation as

$$c_{0m} \cdots c_{kj} c_{ji} c_{ij'} c_{j'k'} \cdots c_{m'0} = \mathrm{I}, \tag{3}$$

where I is the identity map. The LHS of Eq. (3) describes the mapping of cell 0 to itself via a path through cells $m', \ldots, k', j', i, j, k, \ldots, m$ which, as we see, must be the identity mapping. The path, which forms a closed loop that starts and ends in the same cell, here cell 0, satisfies what we call the *loop-imaging condition*: the combination of all optical elements encountered along the loop images every position back to itself.

By choosing the two paths from cell i to cell 0 such that the final segments of both paths are identical, i.e. by choosing paths in which $m = m'$, and multiplying Eq. (3) by c_{0m}^{-1} from the left and by c_{m0}^{-1} from the right, we see that the loop $m \to \cdots \to k' \to j' \to i \to j \to k \to \cdots \to m$ must also satisfy the loop-imaging condition, and the same result can be obtained similarly for any cell and any closed loop in any RTO device, and indeed in any TO device. We call this result the *loop-imaging theorem*.

The loop-imaging theorem holds specifically for closed loops encircling just a single edge in the lens structure (the equivalent statement in 2D is about closed loops encircling an individual vertex), which are the simplest loops that can satisfy the loop-imaging condition non-trivially. Moreover, by combining several such loops into one it is easy to see that if all closed loops encircling any single edge yield the identity mapping, then *any* closed loop will yield the identity mapping as well. This, in turn, implies that the mapping from physical space to virtual space is unique, and that the device therefore satisfies the definition of an RTO device.

We define the *edge-imaging condition* for a particular edge as the requirement that successive imaging by all lenses meeting at the edge yields the identity mapping. In this way, we arrive at a simple formulation of the *edge-imaging theorem*: A lens structure is an RTO device if and only if every edge in the device satisfies the edge-imaging condition. The edge imaging theorem applies equally to structures composed of glenses [15].

3. Example

As an example, consider the structure of 16 ideal thin lenses, each with a triangular clear aperture, shown in Fig. 1(b). The side length of the lens L and the respective heights h_1, h_2, and h of the vertices V_4, V_5, and V_6 above lens L can be chosen arbitrarily as long as $h_1 < h_2 < h$. The lenses divide the interior space of the structure into seven tetrahedral cells; the space between the lenses is empty. In the following, we simply call this structure S.

We arrived at S as a promising candidate for an RTO device in the following way. First, we derived from the edge-imaging condition the following simple necessary conditions on the principal points of lenses meeting at an edge [15]:

1. For edges at which two or three lenses meet, the principal points of all lenses meeting there must coincide.

2. For edges at which four lenses meet, the principal points of all four lenses must lie on a straight line.

Optics EXPRESS

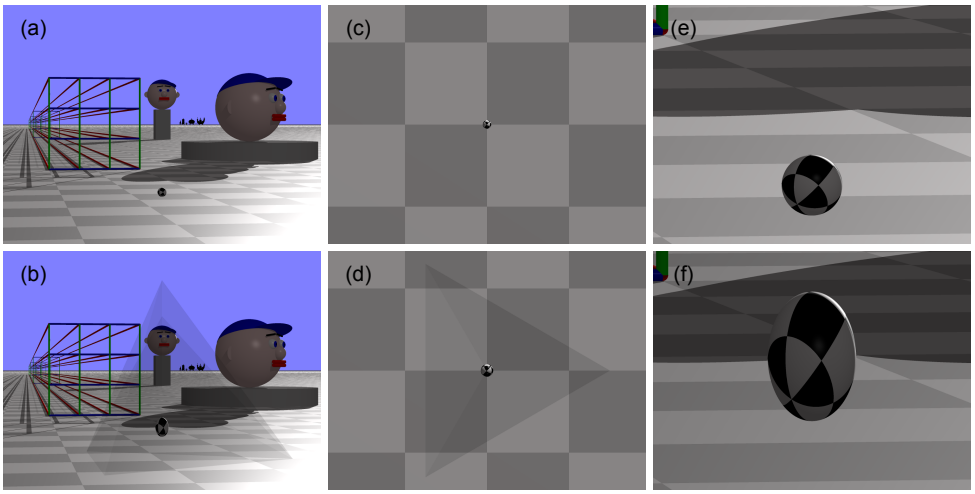

Fig. 2. Simulated visual effect of the ideal-lens structure S (Fig. 1(b)). In the upper images (a, c, e), S is absent, in the lower images (b, d, f) it is present. The left and center columns show the scene from two different viewing positions, from straight above in the case of the center column. The right column shows part of the images in the left column, magnified. The black and white sphere is positioned inside S, the rest of the scene (with the exception of S itself) is outside of S. Any object seen through S appears slightly darker as the ideal lenses that form S have been simulated to be slightly absorptive. The simulations were performed using an extended version of our custom raytracer Dr TIM [16].

Starting with the simplest 2D ideal-lens structure with non-zero inside area, namely a triangle formed by ideal lenses, we added additional ideal lenses until the conditions on the principal points could be satisfied. Finally, we generalised the resulting structure to 3D.

We can use equations derived from the loop-imaging theorem applied to the edges in S to calculate the focal lengths of all lenses from the geometry of S and the focal length of lens L. The tedious calculation of the focal lengths, performed in part using *Mathematica*'s computer algebra, is described in Appendices A and B. Appendix C describes the proof, again performed using *Mathematica*'s computer algebra, that, with the focal lengths calculated in this way, all edges in S satisfy the edge-imaging condition. This proves that the structure S is an RTO device.

Fig. 2 shows raytracing simulations that illustrate the RTO character of S. The images show a scene with and without S, seen from different positions outside S. As discussed in the previous section, in the absence of S all objects are seen in their physical-space positions, in the presence of S they are seen in their virtual-space positions. The mapping between physical space and virtual space distorts only the inside of S, which is why the black and white sphere, which is positioned inside S, appears distorted while the rest of the scene does not. In RTO devices the same virtual space is seen from all outside viewing positions; Fig. 2 confirms this for two outside viewing positions.

The set of equations derived from the edge-imaging condition does not uniquely determine the focal lengths of all lenses in S. One focal length can be chosen arbitrarily; this can, for example, be used to control the virtual-space position of one of the vertices, as has been done in Appendix B. This was also done in the simulations shown in Fig. 2, in which the height of the virtual-space position of V_4 above L was chosen to be twice that of its real-space position. Together with the geometry of S, fixing this degree of freedom completely determines the mapping between physical space and virtual space. An investigation of this mapping is outside the scope of this

Optics EXPRESS

paper; aspects of the mapping are investigated in [13].

Of course, the structure S is only one of many possible ideal-thin-lens RTO devices. For example, and rather trivially, two or more S-type structures can be combined, e.g. one nested inside the other, allowing the number of the degrees of freedom of the mapping between physical space and virtual space to be increased, in principle without limit. More interestingly it should be possible to construct ideal-thin-lens RTO devices with completely different geometries. More calculations are required for such cases, but the loop imaging theorem provides the requisite tool for doing this.

4. Omnidirectional lenses

We now demonstrate that ideal-thin-lens RTO devices have an interesting property: any such device is an *omnidirectional lens*.

To see this, we consider in Fig. 1(b) the cell separated from the outside by the lens L. Let us call this cell, which has vertices V_1 to V_4, cell 1, so the lens L becomes L_{01} in our notation introduced above. Imaging of cell 1 by the lens L_{01} to the outside (cell 0) is then described by the mapping $C_1 = c_{01}$. However, thanks to the loop imaging theorem, exactly the same mapping between cell 1 and the outside is achieved by any other combination of lenses separating cell 1 from the outside. This way, the imaging performed by the rest of the device (i.e. by the structure S with L removed) is exactly the same as imaging by the lens L itself. Therefore the device works as an omnidirectional lens that images between cell 1 and the outside.

An analogous argument can be constructed for any outside lens (not just L_{01}) of any ideal-thin-lens RTO device (not just the structure S). In this sense, any ideal-thin-lens RTO device is an omnidirectional lens.

5. Experimental realisability

Our ideal-thin-lens RTO devices are unusual combinations of ideal thin lenses. Lenses are essentially paraxial instruments, and as ideal thin lenses are normally used as convenient approximations to real lenses, they are normally used paraxially. We chose not to be constrained by paraxiality here, which opens up potential applications, which we discuss below, but which also raises questions about the realisability of our devices.

Lenses, in particular thick lenses, do not work well non-paraxially, which suggests that realisations of ideal-thin-lens-RTO devices in terms of standard lenses (i.e. ideal-thin-lens RTO devices in which each ideal thin lens has been replaced with a corresponding standard lens) are unlikely to work. We have confirmed this with a number of raytracing simulations through detailed glass structures that correspond to such real-lens realisations of ideal-thin-lens RTO devices: if each ideal thin lens is replaced by a corresponding symmetric lens, the simulated view through such devices (not shown) looks very different from that through the corresponding ideal-thin-lens devices. We also simulated realisations of our devices in terms of phase holograms of lenses, designed such that they image, in principle stigmatically, between points on the optical axis a distance $2f$ on either side of the hologram. These simulated phase-hologram devices also look nothing like the corresponding ideal-thin-lens structures.

However, phase holograms can be designed to image, again in principle stigmatically, between any *one* pair of conjugate positions: at any point on the hologram, the hologram simply has to shift the phase of transmitted light such that the phase of light that travels in a straight line from the object position to the point on the hologram and from there to the image position becomes independent of the position on the hologram. (Note that standard lenses, including Fresnel lenses, can be similarly optimised for specific object-image pairs.) When applied to our devices, this allows us to design the constituent phase holograms such that the resulting device works perfectly for light rays that pass through one particular position, for example for one particular viewing position, in which case the device is, of course, no longer omnidirectional.

Optics EXPRESS

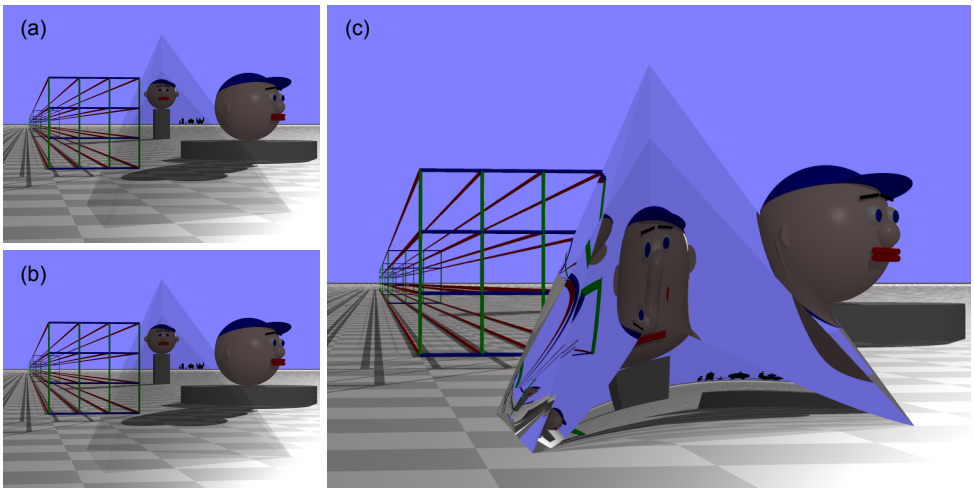

Fig. 3. Raytracing simulations of a phase-hologram realisation of the ideal-lens structure S shown in Fig. 2. When seen from the intended viewing position (a), the device does not distort the scene seen through it, exactly like the corresponding ideal-thin-lens device (b). This is not the case for any other viewing position; an example is shown in (c). The light-ray-direction change due to each hologram was calculated by treating each ray as a plane wave, adding the transverse phase gradient introduced by the hologram to the transverse wave numbers, and calculating the longitudinal wave number such that each plane wave retains its wavelength (i.e. such that $k_x^2 + k_y^2 + k_z^2 = (2\pi/\lambda)^2$) — see [17] below Eq. (21). All simulations assumed perfect dispersion compensation for all visible light and were performed with an extended version of our custom raytracer Dr TIM [16].

Above, we found that there is a unique mapping, C_i, from the space of cell i to the exterior of the device: any position V_i in the space of cell i is mapped to a position in the outside space, cell 0, $\mathrm{V}_0 = C_i \mathrm{V}_i$. Conversely, the outside-space position V_0 is of course mapped to the position in the space of cell i: $\mathrm{V}_i = C_i^{-1} \mathrm{V}_0$. If we now choose V_0 to be the viewing position, we can see that the ideal thin lens L_{ij} separating cells i and j images the positions V_i and V_j into each other. Now all we need to do is design the phase hologram replacing L_{ij} such that it, too, images between V_i and V_j. If we design all phase holograms in the device in this way, then, for viewing position V_0 (and for this position only), the device distorts the view *exactly* as it would if it consisted of ideal thin lenses (Fig. 3).

The development of this new application for lens holograms coincides with rapid advances in the development of efficient phase (and amplitude) holograms in the form of metasurfaces [18–23]. A realisation of holograms in the form of metasurfaces has a number of advantages over previous incarnations, for example enabling compensation of dispersion effects [24, 25]. Metasurfaces have already been used to build novel lenses [26–28], and there is an expectation that these developments will result in better real-life-approximations to ideal thin lenses.

6. Potential applications

Lenses are amongst the oldest, simplest, and most widely used optical components. Improving an aspect of lenses, as an omnidirectional lens does by increasing the field of view (FOV) to the largest possible value, could therefore potentially have wide-ranging applications. Below we list a few potential applications omnidirectional lenses, or parts thereof. All of these applications have the property that either the observer's eye pupil or the object are located near a particular

Optics EXPRESS

position, which means it should be possible to realise the proposed devices such that they work around those positions.

One application where an enlarged subtended FOV might find use is in microscopy, where the resolution depends on the solid angle over which the objective lens collects light from the sample. This solid angle is normally limited to 2π; this limit can be approached by placing a microscope objective very close to the sample. When light is collected over (nearly) the entire 4π solid angle, like in "4pi microscopes" that use two objectives placed close to the sample [29], the axial resolution can be improved. This could, perhaps and perhaps better, alternatively be achieved with omnidirectional lenses.

A second potential application for lenses with an enlarged FOV is in virtual-reality (VR) headsets. VR headsets are currently a vast and growing market, but they suffer from a number of imperfections that prevent the viewer from experiencing complete immersion. One of these imperfections is limited FOV: many current VR headsets give the impression of looking at a scene through binoculars. A suitable section of an omnidirectional lens that allows the generated view to fill the observer's entire visual field could add to existing solutions (such as [30]).

A third potential application is image rotation. Our primary motivation is that, in patients with cyclodeviation, the brain cannot compensate for a rotational misalignment of the eyeballs around a forward axis, leading to double vision [31]. Currently, there is no standard treatment for small rotation angles, and for larger angles surgery is the only treatment option, largely because there exist currently no compact optical image-rotation devices with a large enough FOV. We noticed that, in raytracing simulations of the view out of one of the inner cells of the structure S, the view in a particular direction appeared rotated. (The view out of any of the outer cells is always that through an omnidirectional lens, and does not appear rotated.) The view is through a combination of three skew lenses, and such combinations might therefore be suitable for the treatment of cyclodeviation.

7. Conclusions

We have shown here that structures of ideal thin lenses can form novel RTO devices that can be interpreted as omnidirectional lenses. We have supported our calculations with detailed raytracing simulations.

The standard design process for a TO device starts with the desired mapping between physical space and virtual space, from which the corresponding material parameters are then calculated. We used a very different design process to arrive at our example for an omnidirectional ideal-lens RTO device, the structure S: we started with a process of elimination based on the edge-imaging theorem to find a candidate ideal-lens structure, specifying the planes of all lenses and the positions of their principal points; we applied the edge-imaging condition to each edge in S to derive the relationship between the focal lengths of all lenses; and finally we solved those relationships for all focal lengths, and showed that, with this set of focal lengths, *all* focal-length relationships were satisfied. According to the edge-imaging theorem, this then showed that S is an omnidirectional RTO device. Once the physical-space geometry of S is fixed, there is a single degree of freedom in the choice of the focal lengths, providing limited control over the mapping between physical space and virtual space; all other aspects of this mapping are then fixed. The calculations involved in finding the focal lengths were lengthy, which is why we performed them with the help of computer algebra. Future work should aim to develop a less arduous design process; at the very least, it should be possible to automate completely the calculation of the focal lengths from the geometry of the lens structure. This will allow more complex structures to be considered, which in turn will provide increased control over the mapping between physical space and virtual space.

With compromises, it should be possible to realise such devices experimentally. We have shown raytracing simulations which fully take into account the light-ray-direction change that

Optics EXPRESS

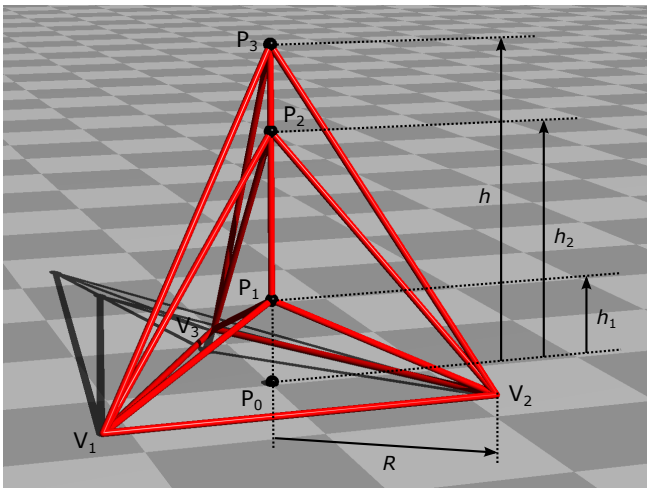

Fig. 4. Structure and parameters of the ideal-lens structure S. The red tubes indicate the edges of ideal thin lenses; each triangle formed by red tubes is the aperture of a lens, of which there are 16 in total. The lenses form a structure that can be understood as three nested tetrahedra that share a base (an equilateral triangle with vertices V_1, V_2 and V_3, centered at P_0, and with circumradius R), but that have different heights, respectively h_1 (the tetrahedron with fourth vertex P_1), h_2 (fourth vertex P_2), and h (the outermost tetrahedron with fourth vertex P_3). Black spheres are centered on the positions P_0 to P_3, which are the positions of the principal points of the lenses. (Note that the principal point coincides with the aperture center only in the base lens.) The vertical line through the principal points is an axis of three-fold symmetry.

can be achieved with phase holograms or metalenses, assuming perfect dispersion compensation and neglecting reflection and transmission losses, conditions that we expect future metalenses to meet increasingly well.

Our results provide strong motivation for attempting an experimental realisation of an omnidirectional lens, for working towards a better understanding of skew-lens devices, and for investigating further potential applications of this novel technology.

Appendix A. Loop-imaging-theorem equations for different intersection geometries

Fig. 4 defines the parameters we use to describe the geometry of the ideal-lens structure S. The lens intersections in the ideal-lens structure can be divided into three types, sketched on the left-hand side of Fig. 5. To the right of each sketch is a raytracing image that shows a cylinder-frame model of the ideal-lens structure in which the edges with the sketched geometry are highlighted.

We describe all intersection geometries in a coordinate system in which the intersection line coincides with the z axis. We calculate the position of the image $\mathbf{Q}'$ of an object at position $\mathbf{Q}$ due to an individual lens with focal length f, principal-point position $\mathbf{P}$, and (normalised) optical-axis direction $\hat{\mathbf{a}}$, according to the equation

$$\mathbf{Q}' = \mathbf{Q} + \frac{(\mathbf{Q}-\mathbf{P})\cdot\hat{\mathbf{a}}}{f-(\mathbf{Q}-\mathbf{P})\cdot\hat{\mathbf{a}}}(\mathbf{Q}-\mathbf{P}), \tag{4}$$

which is Eq. (3) in [11], applied to the special case of a lens.

We now apply the loop-imaging theorem to all three lens-intersection types in turn.

Optics EXPRESS

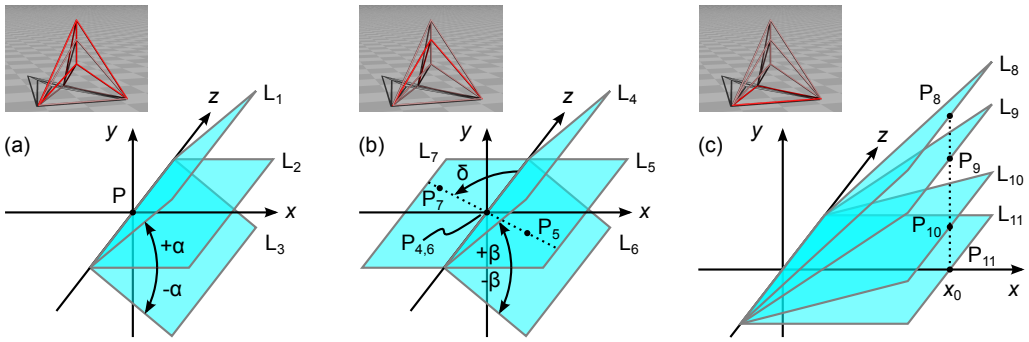

Fig. 5. Application of the loop-imaging theorem to the edges in the ideal-lens structure. Each row corresponds to one edge geometry. The drawings sketch the edge geometries, indicating a suitable choice of coordinate system and the parameters. The raytracing images above the drawings show a cylinder-frame model of the ideal-lens structure highlighting (in red) the edges that possess the geometry shown in the corresponding drawing. (a) Three lenses, L_1 to L_3, intersect such that the angle from L_2 to L_1 is equal in magnitude but opposite in sign to the angle from L_2 to L_3. All three lenses share a common principal point, P, which lies on the intersection. (b) Four lenses, L_4 to L_7, intersect such that L_5 and L_7 lie in the same plane but on opposite sides of the intersection line, and L_4 and L_6 are arranged symmetrically with respect to this plane. The principal points lie on a straight line in the plane of L_5 and L_7. This straight line makes an angle δ with the intersection line. (c) Four lenses, L_8 to L_{11}, intersect. The principal points lie on a straight line that is perpendicular to the plane of L_{11}. In all drawings, the coordinate system is chosen such that the lenses intersect along the z axis. In (a), the x axis was chosen such that the (x, z) plane is the plane of mirror symmetry.

A.1. Mirror-symmetric three-lens intersection

We start with the symmetric arrangement of three lenses shown in Fig. 5(a). The three lenses share a principal point, P, that lies on the intersection line. We choose to place the origin of the coordinate system at P. We choose the direction of the x axis such that the second lens, L_2, lies in the (x, z) plane. The other two lenses, L_1 and L_3, make angles $+\alpha$ and $-\alpha$ with L_2. L_1 and L_3 have the same focal length, f_1; the focal length of L_2 is f_2.

We start with an arbitrary position $\mathbf{Q} = (x, y, z)$ and calculate the position $\mathbf{Q}'$ to which successive imaging by L_1, L_2 and L_3 maps $\mathbf{Q}$. The result, calculated in Mathematica, is

$$\mathbf{Q}' = \frac{f_1 f_2}{d}\mathbf{Q}, \tag{5}$$

where

$$d = f_1(f_2 - y) - 2f_2 y\cos\alpha. \tag{6}$$

In order for the position of the image produced by the combination of the three lenses, $\mathbf{Q}'$, to equal the object position, $\mathbf{Q}$, we require $\mathbf{Q}' = \mathbf{Q}$, or $\mathbf{Q}' - \mathbf{Q} = 0$, or, provided $d \neq 0$ (which we will confirm below), $d\,(\mathbf{Q}' - \mathbf{Q}) = 0$. With the definition

$$Z = d\,(\mathbf{Q}' - \mathbf{Q}), \tag{7}$$

we then require $Z = 0$. Note that we have multiplied $\mathbf{Q}' - \mathbf{Q}$ by d to ensure that the resulting expression, Z, is a polynomial in x, y and z. We require the polynomial Z in x, y and z to be zero for any object position, that is, for any combination of x, y and z. This implies that every single coefficient in the polynomial is individually zero. The only non-zero coefficients are all of

Optics EXPRESS

the form $f_1 + 2f_2 \cos\alpha$, and so the focal lengths are related through the equation

$$f_1 + 2f_2 \cos\alpha = 0. \tag{8}$$

To show that $d \neq 0$, which is an assumption we made above, we solve Eq. (8) for f_1 and substitute the result into the expression for d, which becomes $d = -2f_2^2 \cos\alpha$. This expression is non-zero provided that $f_2 \neq 0$ (which is the case in all physically meaningful situations) and $\cos\alpha \neq 0$, i.e. $\alpha \neq \pm\pi/2, \pm 3\pi/2, \pm 5\pi/2, \ldots$, which is the case in the cases we are interested in.

This result allows us to link the focal lengths of all 3-lens edges in the structure. Note that at the vertical edges the angles between neighbouring lenses are $2\pi/3$. Substituting $\alpha = 2\pi/3$ into Eq. (8) gives $f_1 = f_2$, i.e. all lenses meeting at the vertical edges are identical. We require this for symmetry, so this result is reassuring.

The full calculation is contained in the *Mathematica* notebook `3LensIntersection.nb` [32].

A.2. Mirror-symmetric four-lens intersection

Fig. 5(b) shows the geometry of 4-lens edges. The structure is mirror-symmetric with respect to the common plane of lenses L_5 and L_7. Additionally, all principal points lie on a straight line through the origin in the (x, z) plane at an angle δ to the z axis; P_4 and P_6 lie on the origin, P_5 and P_7 respectively lie distances h_5 and h_7 from the origin.

Using the same approach as above, we find that, for $h_5 \neq h_7$ and $h_7 \neq 0$,

$$\frac{f_5}{f_7} = \frac{h_5}{h_7}, \quad f_4 = \frac{f_7(2f_5 \cos\beta + h_5 \sin\beta \sin\delta)}{f_5 - f_7}. \tag{9}$$

In the special case $h_5 = h_7 \neq 0$,

$$f_5 = f_7 = -\frac{h_7}{2} \sin\delta \tan\beta. \tag{10}$$

The full calculation is contained in the *Mathematica* notebook `4LensIntersection.nb` [32].

A.3. Asymmetric four-lens intersection

In the final geometry, the z axis is the edge of four lenses, L_8 to L_{11}. The coordinate system is chosen such that lens L_{11} lies in the $y = 0$ plane. The principal points of all four lenses lie on a straight line parallel to the y axis (i.e. perpendicular to lens L_{11}) that intersects the x axis at $x = x_0$. This geometry is sketched in Fig. 5(c).

We call the y component of the principal point of lens L_i y_i; that principal point is then located at position $(x_0, y_i, 0)$. We call the angle between lens L_i and the xz-plane φ_i; it holds $y_i = x_0 \tan\varphi_i$.

To find the conditions for the focal lengths of the lenses, we use the following fact that follows from the loop theorem in a straightforward way: if some point A in the cell between lenses L_9 and L_{10} is imaged successively by lenses L_9 and L_8, the resulting image (call it $A_{9,8}$) must be located at the same point as if point A is imaged successively by lenses L_{10} and L_{11} (call the corresponding image $A_{10,11}$). The requirement $A_{10,11} = A_{9,8}$ then yields certain conditions for the focal lengths of the four lenses. The same argument can then be applied to a point B in the cell between lenses L_{10} and L_{11}; its image $B_{10,9,8}$ by lenses L_{10}, L_9 and L_8 must be identical to the image B_{11} by lens L_{11}. This yields additional conditions for the focal lengths.

To find these conditions, we choose the point A (and later also B) in a special way, namely such that A lies at the intersection (call it $l_{9,10}$) of the focal planes of lenses L_9 and L_{10} (Fig. 6). Since A lies in both of these focal planes, rays emerging from A and reaching the cell between lenses L_9 and L_8 form a parallel bundle, and the same is true for rays emerging from A and reaching the

Optics EXPRESS

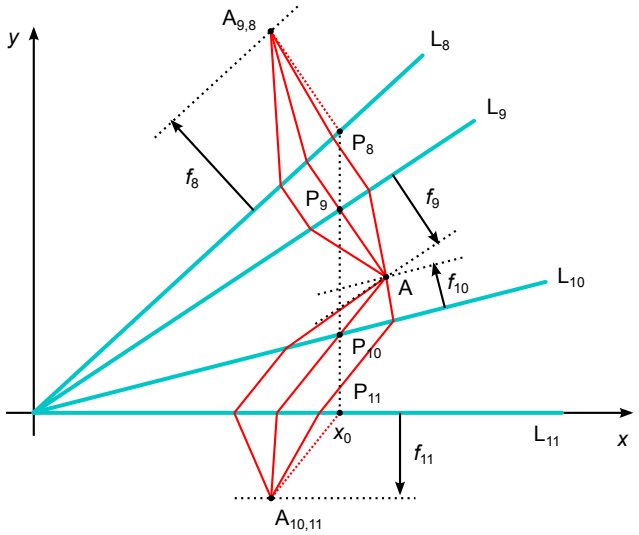

Fig. 6. Placement of the point A in the space between lenses L_9 and L_{10} and construction of two images of A, namely $A_{9,8}$, the image due to lenses L_9 and L_8, and $A_{10,11}$, that due to L_{10} and L_{11}. A lies on the intersection between the focal planes of lenses L_9 and L_{10}. For the four lenses to satisfy the loop-imaging-theorem condition, the locations of the images $A_{9,8}$ and $A_{10,11}$ have to coincide.

cell between lenses L_{10} and L_{11}. The image $A_{10,11}$ can then be found easily: it lies in the focal plane of lens L_{11} because it is a result of focusing of a parallel bundle, and the precise position within this plane can be found by employing a ray from the above mentioned parallel bundle between lenses L_{10} and L_{11} that passes through the principal point P_{11} of lens L_{11}. This ray (call it $m_{10,11}$) is not deflected by lens L_{11}, so point $A_{10,11}$ lies at the intersection of this ray and the focal plane of lens L_{11}. In a similar way the position of the image point $A_{9,8}$ can be found.

To put this into equations, we first write down several general formulas that will be useful. The axis of lens L_i (which is in fact perpendicular to the line $y_i = x_0 \tan\varphi_i$) can be parametrized as

$$(x, y, z) = (x_0 - t\sin\varphi_i, y_0 + t\cos\varphi_i, 0), \tag{11}$$

where t is a real parameter. Then, we can find focal planes very easily by substituting $t = \pm f_i$ in Eq. (11). The upper and lower sign corresponds to the "upper" and "lower" focal plane, respectively. Applying the fact that focal planes are parallel to the plane of a lens, the focal planes can then be parametrized as

$$(x, y, z) = (x_0 \mp f_i\sin\varphi_i + t\cos\varphi_i, y_i \pm f_i\cos\varphi_i + t\sin\varphi_i, s), \tag{12}$$

where t, s are real parameters as well. Eq. (12) can equivalently be written as

$$(y - y_i) = (x - x_0)\tan\varphi_i \pm F_i, \tag{13}$$

where we have denoted $F_i \equiv f_i/\cos\varphi_i$. As we have mentioned, we place point A at the intersection of focal planes of lenses L_9 and L_{10}. In particular, it is the intersection of the lower focal plane of lens L_9 and upper focal plane of lens L_{10}. Writing Eq. (13) for lenses L_9 and L_{10} with the appropriate signs, using the fact that $y_i = x_0\tan\varphi_i$ and equating them, we get the parametric equations of the line $l_{9,10}$ as

$$x = \frac{F_9 + F_{10}}{\tan\varphi_9 - \tan\varphi_{10}} \equiv x_{9,10}, \quad y = \frac{F_9\tan\varphi_{10} + F_{10}\tan\varphi_9}{\tan\varphi_9 - \tan\varphi_{10}} \equiv y_{9,10}, \quad z = t\,. \tag{14}$$

Optics EXPRESS

We have denoted the values of the x and y coordinates of this line by $x_{9,10}$ and $y_{9,10}$, respectively.

Now, point A can be any point whose coordinates satisfy Eqs (14). We choose this point by fixing the value of the parameter t to t_0. The ray aiming from point A to the principal point of lens L_{10} will not be deflected by this lens, so the direction of this ray determines the direction of the parallel bundle in the cell between lenses L_{10} and L_{11}. It is obvious that the line passing through both points A and P_{10} can be parametrized in the following way:

$$x = x_0 + t(x_{9,10} - x_0), \quad y = y_{10} + t(y_{9,10} - y_{10}), \quad z = t + t_0\,. \tag{15}$$

The above mentioned ray $m_{10,11}$ (a ray from the parallel bundle between lenses L_{10} and L_{11} that passes through the principal point P_{11} of lens L_{11}) can therefore be obtained by paralelly shifting the line parametrized by Eq. (15) such that it passes through the principal point P_{11}. Doing this, we get the equations of the line $m_{10,11}$ as

$$x = x_0 + t(x_{9,10} - x_0), \quad y = y_{11} + t(y_{9,10} - y_{10}), \quad z = t + t_0\,. \tag{16}$$

In a similar way we can find the analogous line $m_{9,8}$ on which the image $A_{9,8}$ of point A by lenses L_9 and L_8 must be located:

$$x = x_0 + s(x_{9,10} - x_0), \quad y = y_8 + s(y_{9,10} - y_9), \quad z = s + t_0\,. \tag{17}$$

Now, since the images $A_{9,8}$ and $A_{10,11}$ must coincide, the lines $m_{9,8}$ and $m_{10,11}$ should actually intersect (so they should not miss each other) and their intersection, point $A_{9,8} = A_{10,11}$, must lie at the intersection of focal planes of lenses L_8 and L_{11}. Equating the pairs of Eqs (16) and (17), we can easily verify that they are compatible, so the straight lines $m_{9,8}$ and $m_{10,11}$ indeed do intersect. Denoting the x and y coordinates of their intersection point $A_{9,8} = A_{10,11}$ by $x_{8,11}$ and $y_{8,11}$ (we will not need the coordinate z), we get

$$x_{8,11} = x_0\frac{\tan\varphi_8 - \tan\varphi_9 + \tan\varphi_{10} - \tan\varphi_{11}}{\tan\varphi_{10} - \tan\varphi_9} + \frac{\tan\varphi_8 - \tan\varphi_{11}}{(\tan\varphi_{10} - \tan\varphi_9)^2}\,(F_9 + F_{10})\,, \tag{18}$$

$$y_{8,11} = x_0\frac{\tan\varphi_8\tan\varphi_{10} - \tan\varphi_9\tan\varphi_{11}}{\tan\varphi_{10} - \tan\varphi_9} + \frac{\tan\varphi_8 - \tan\varphi_{11}}{(\tan\varphi_{10} - \tan\varphi_9)^2}\,(F_9\tan\varphi_{10} + F_{10}\tan\varphi_9)\,. \tag{19}$$

As has been mentioned, this intersection point must lie in the focal planes of both lenses L_8 and L_{11}. Finding the intersection line of these focal planes in the same way as we found the intersection line of focal planes of lenses L_9 and L_{10} before, see Eq. (14), we find for the coordinates $x_{8,11}$ and $y_{8,11}$

$$x_{8,11} = \frac{F_8 + F_{11}}{\tan\varphi_{11} - \tan\varphi_8}, \quad y_{8,11} = \frac{F_8\tan\varphi_{11} + F_{11}\tan\varphi_8}{\tan\varphi_{11} - \tan\varphi_8}\,. \tag{20}$$

Now, equating the $x_{8,11}$ and $y_{8,11}$ from Eqs (20) with their values expressed by Eqs (18) and (19) gives two conditions for the parameters F_8, F_9, F_{10}, F_{11} (which imply the conditions for the focal lengths) in the form of two inhomogeneous linear equations:

$$\frac{F_8 + F_{11}}{y_{11} - y_8} = \frac{-y_8 + y_9 - y_{10} + y_{11}}{y_9 - y_{10}} + \frac{y_8 - y_{11}}{(y_9 - y_{10})^2}\,(F_9 + F_{10})\,, \tag{21}$$

$$\frac{F_8 y_{11} + F_{11} y_8}{y_{11} - y_8} = \frac{y_{11}y_9 - y_8 y_{10}}{y_9 - y_{10}} + \frac{y_8 - y_{11}}{(y_9 - y_{10})^2}\,(F_9 y_{10} + F_{10} y_9)\,. \tag{22}$$

Writing these equations, we have employed the fact that $x_0\tan\varphi_i = y_i$. Repeating the completely analogous procedure with a point B in the cell between lenses L_{10} and L_{11}, at the intersection of

Optics EXPRESS

their focal planes (line $l_{10,11}$), we get two additional inhomogeneous linear equations:

$$\frac{F_9 + F_8}{y_8 - y_9} = \frac{y_8 - y_9 + y_{10} - y_{11}}{y_{10} - y_{11}} + \frac{y_9 - y_8}{(y_{10} - y_{11})^2}(F_{10} + F_{11}), \tag{23}$$

$$\frac{F_9 y_8 + F_8 y_9}{y_8 - y_9} = \frac{y_8 y_{10} - y_9 y_{11}}{y_{10} - y_{11}} + \frac{y_9 - y_8}{(y_{10} - y_{11})^2}(F_{10} y_{11} + F_{11} y_{10}). \tag{24}$$

In total we then have a set of four linear inhomogeneous equations for four unknowns F_8, F_9, F_{10}, F_{11}. We have solved this set with the program Mathematica, which revealed that the equations are actually linearly dependent, allowing to choose one of the parameters (e.g. F_{11}) arbitrarily and express the other three in terms of it. This yields the following expressions for the focal lengths:

$$\begin{aligned} f_8 &= f_{11}\frac{s_{11}\Delta y_{8,9}\Delta y_{8,10}}{s_8\Delta y_{9,11}\Delta y_{11,10}} + \frac{x_0\Delta y_{8,9}\Delta y_{8,11}}{s_8\Delta y_{9,11}}, \quad f_9 = -f_{11}\frac{s_{11}\Delta y_{8,9}\Delta y_{9,10}}{s_9\Delta y_{8,11}\Delta y_{11,10}}, \\ f_{10} &= f_{11}\frac{s_{11}\Delta y_{8,10}\Delta y_{9,10}}{s_{10}\Delta y_{8,11}\Delta y_{11,9}} - \frac{x_0\Delta y_{10,9}\Delta y_{10,11}}{s_{10}\Delta y_{9,11}}, \end{aligned} \tag{25}$$

where $\Delta y_{i,j} = y_i - y_j$ and $s_i = \sqrt{x_0^2 + y_i^2}$.

This way, we have found the necessary conditions for the focal lengths f_8, f_9, f_{10}, f_{11} such that the points A lying on the line $l_{9,10}$ described above are imaged equally by lenses L_9 and L_8 as by lenses L_{10} and L_{11}, and points B lying on the line $l_{10,11}$ are imaged equally by lenses L_{10}, L_9 and L_8 as by lens L_{11}. What still needs to be shown is that this is already also the sufficient condition, i.e., that *any* point A in the cell between lenses L_9 and L_{10} is imaged the same way by the two lens combinations.

To show that it is indeed true, we note that there are three straight lines in the cell 0 (the outer region outside of the lenses L_8 and L_{11}), the points on each of them being imaged to themselves by the lens combination L_8, L_9, L_{10} and L_{11}. In other words, a ray aiming to any point on any of these three lines, when it passes successively through the lenses L_8, L_9, L_{10} and L_{11}, continues in the same direction and the same transversal position as if it had not passed through the lenses at all. These three lines are the following: the first one is the z-axis; since is lies in the planes of all four lenses, each of its point is imaged to itself by each lens separately, and the same is therefore true for the lens combination. The second line is the image of line $l_{9,10}$ by lenses L_9 and L_8, or, equivalently, by L_{10} and L_{11}—precisely because these two lens combinations image the points on line $l_{9,10}$ the same way. The third line is the image of line $l_{10,11}$ by the lens combination L_{10}, L_9 and L_8, or by lens L_{11} alone, again for the same reason. This line lies at infinity because lens L_{11} changes rays emerging from a point B $\in l_{10,11}$ into a parallel bundle. So we have now three straight lines (all parallel to the z-axis) whose imaging by the lenses L_8, L_9, L_{10} and L_{11} is given by the identity mapping. Apart from the degenerate case when these lines all lie in one plane, it then follows that the collineation given by imaging by lenses L_8, L_9, L_{10} and L_{11} must be identity mapping for the whole space. This completes the proof that the loop theorem assumptions are fulfilled by the four-lens edge in our device.

Appendix B. Calculation of the focal lengths

We can use the results obtained in the previous section to calculate, for a given physical-space structure and a given virtual-space position of the lower inner vertex, all focal lengths in the ideal-lens structure, as follows.

The focal length f_D of the base lens, lens D in Fig. 7, is fully determined by the position of the lower inner vertex in physical space and electromagnetic space, as the base lens images these into each other. If h_1' is the height above the base lens of the lower inner vertex in virtual space,

Optics EXPRESS

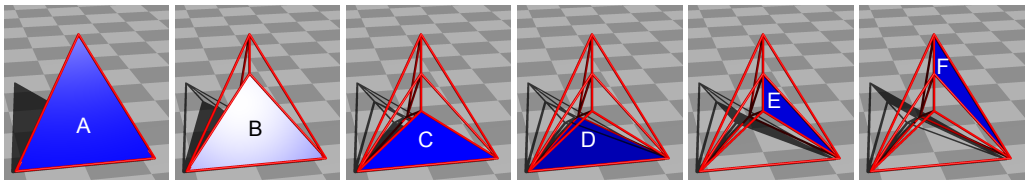

Fig. 7. The different types of ideal lenses that make up the ideal-lens structure. Each frame shows a solid triangle in the plane of one of the corresponding lenses. As the ideal-lens structure is 3-fold rotationally symmetric around the vertical axis of the structure, there are three lenses of all types other than type D, of which there is only one lens.

then application of the lens equation yields

$$f_{\mathrm{D}} = \frac{h_1 h_1'}{h_1' - h_1}. \tag{26}$$

Below, we will express all other focal lengths in terms of f_{D}.

At each of the bottom edges of the ideal-lens structure, four lenses of type A, B, C and D intersect such that their focal lengths are described by Eqns (25) when f_{A} is substituted for f_8, f_{B} for f_9, f_{C} for f_{10}, f_{D} for f_{11}, h_1 for y_{10} h_2 for y_9, h for y_8, and $R/2$ for x. The solution is

$$\begin{aligned} f_{\mathrm{A}} &= -\frac{(h_2 - h)\,(f_{\mathrm{D}}(h_1 - h) + h_1 h)\,R}{h_1 h_2 \sqrt{4h^2 + R^2}}, \quad f_{\mathrm{B}} = \frac{f_{\mathrm{D}}(h_1 - h_2)(h_2 - h)R}{h_1 h \sqrt{4h_2^2 + R^2}}, \\ f_{\mathrm{C}} &= -\frac{(h_1 - h_2)\,(f_{\mathrm{D}}(h_1 - h) + h_1 h)\,R}{h_2 h \sqrt{4h_1^2 + R^2)}}. \end{aligned} \tag{27}$$

The focal length of the upper vertical lenses, f_{F}, can then be calculated from Eq. (8) with the substitutions $f_1 \to f_{\mathrm{A}}$, $f_2 \to f_{\mathrm{F}}$, and $\cos\alpha \to -\hat{\mathbf{a}}_{\mathrm{F}} \cdot \hat{\mathbf{a}}_{\mathrm{A}}$, and that of the lower vertical lenses, f_{E}, using the first equation in (9) with the substitutions $f_5 \to f_{\mathrm{E}}$, $f_7 \to f_{\mathrm{F}}$, $h_5 \to h_1 - h_2$, and $h_7 \to h - h_2$. The resulting focal lengths are

$$f_{\mathrm{E}} = -\frac{(h_1 - h_2)\,(f_{\mathrm{D}}(h_1 - h) + h_1 h)\,R}{2\sqrt{3} h_1 h_2 h}, \quad f_{\mathrm{F}} = \frac{(h_2 - h)\,(f_{\mathrm{D}}(h_1 - h) + h_1 h)\,R}{2\sqrt{3} h_1 h_2 h}. \tag{28}$$

The detailed calculations can be found in the *Mathematica* document `allLoopTheorems.nb` [32].

Appendix C. With the correct choice of focal lengths, S is a transformation-optics device

In the calculation of the focal lengths in the previous section, we have not yet used the second equation in (9), which needs to be satisfied with the substitutions $f_4 \to f_{\mathrm{B}}$, $f_5 \to f_{\mathrm{E}}$, $f_7 \to f_{\mathrm{F}}$, $h_5 \to h_1 - h_2$, $\beta \to -\cos^{-1}(-\hat{\mathbf{a}}_{\mathrm{B}} \cdot \hat{\mathbf{a}}_{\mathrm{E}})$, and with δ replaced with its value as calculated from the geometry for the device to be consistent. We have also not used the loop-imaging theorem for the lower inner edges in Fig. 5(a), i.e. Eq. (8) with the substitutions $f_1 \to f_{\mathrm{C}}$, $f_2 \to f_{\mathrm{E}}$, $\cos\alpha \to \hat{\mathbf{a}}_{\mathrm{E}} \cdot \hat{\mathbf{a}}_{\mathrm{C}}$.

It can be shown that the expressions for the focal lengths found in the previous section also satisfy these missing equations. We have done this in the *Mathematica* document `allLoopTheorems.nb` [32]. This proves that, with the right choice of focal lengths, all edges in the ideal-lens structure satisfy the loop-imaging theorem, and that therefore, by the edge-imaging theorem, the ideal-lens structure S is an RTO device.

Optics EXPRESS

Funding

Engineering and Physical Sciences Research Council (EPSRC) (EP/K503058/1, EP/M010724/1); Grantová Agentura České Republiky (GAČR) (P201/12/G028).

Acknowledgments

We acknowledge helpful discussions with Jörg Courtial (Faber Courtial GbR, Darmstadt, Germany) and Hari Prasad (The Perse School, Cambridge, UK).

References

1. U. Leonhardt, "Optical conformal mapping," Science **312**, 1777–1780 (2006).
2. J. B. Pendry, D. Schurig, and D. R. Smith, "Controlling electromagnetic fields," Science **312**, 1780–1782 (2006).
3. F. Monticone and A. Alù, "Invisibility exposed: physical bounds on passive cloaking," Optica **3**, 718–724 (2016).
4. H. Chen, B. Zheng, L. Shen, H. Wang, X. Zhang, N. Zheludev, and B. Zhang, "Ray-optics cloaking devices for large objects in incoherent natural light," Nature Commun. **4**, 2652 (2013).
5. J. S. Choi and J. C. Howell, "Digital integral cloaking," Optica **3**, 536–540 (2016).
6. G. Lippmann, "La photographie intégrale," C. R. Hebd. Acad. Sci. **146**, 446–451 (1908).
7. J. S. Choi and J. C. Howell, "Paraxial ray optics cloaking," Opt. Express **22**, 29465–29478 (2014).
8. S. Oxburgh, C. D. White, G. Antoniou, E. Orife, and J. Courtial, "Transformation optics with windows," Proc. SPIE **9193**, 91931E (2014).
9. S. Oxburgh, C. D. White, G. Antoniou, E. Orife, T. Sharpe, and J. Courtial, "Large-scale, white-light, transformation optics using integral imaging," J. Opt. **18**, 044009 (2016).
10. T. Tyc, S. Oxburgh, E. N. Cowie, G. J. Chaplain, G. Macauley, C. D. White, and J. Courtial, "Omni-directional transformation-optics cloak made from lenses and glenses," J. Opt. Soc. Am. A **33**, 1032–1040 (2016).
11. G. J. Chaplain, G. Macauley, J. Bělín, T. Tyc, E. N. Cowie, and J. Courtial, "Ray optics of generalized lenses," J. Opt. Soc. Am. A **33**, 962–969 (2016).
12. S. Oxburgh and J. Courtial, "Perfect imaging with planar interfaces," J. Opt. Soc. Am. A **30**, 2334–2338 (2013).
13. J. Courtial, S. Oxburgh, E. N. Cowie, C. D. White, and T. Tyc, "Omni-directional cloaking using ideal lenses," in preparation (2018).
14. D. S. Goodman, "General principles of geometric optics," in "Handbook of Optics. Volume I: Fundamentals, Techniques, and Design," 2nd ed., M. Bass, E. W. V. Stryland, D. R. Williams, and W. L. Wolfe, eds. (McGraw-Hill, 1995), chap. 1.15, pp. 1.60–1.68.
15. T. Tyc, S. Oxburgh, C. D. White, E. N. Cowie, and J. Courtial, "On the loop-imaging theorem of transformation optics," in preparation (2018).
16. S. Oxburgh, T. Tyc, and J. Courtial, "Dr TIM: Ray-tracer TIM, with additional specialist capabilities," Comp. Phys. Commun. **185**, 1027–1037 (2014).
17. J. Courtial and T. Tyc, "Generalised laws of refraction that can lead to wave-optically forbidden light-ray fields," J. Opt. Soc. Am. A **29**, 1407–1411 (2012).
18. N. Yu, P. Genevet, M. A. Kats, F. Aieta, J.-P. Tetienne, F. Capasso, and Z. Gaburro, "Light propagation with phase discontinuities: Generalized laws of reflection and refraction," Science **334**, 333–337 (2011).
19. X. Ni, A. V. Kildishev, and V. M. Shalaev, "Metasurface holograms for visible light," Nature Communications **4**, 2807 (2013).
20. N. Yu and F. Capasso, "Flat optics with designer metasurfaces," Nat. Mater. **13**, 139 (2014).
21. G. Zheng, H. Mühlenbernd, M. Kenney, G. Li, T. Zentgraf, and S. Zhang, "Metasurface holograms reaching 80% efficiency," Nat. Nanotech. **10**, 308 (2015).
22. L. Wang, S. Kruk, H. Tang, T. Li, I. Kravchenko, D. N. Neshev, and Y. S. Kivshar, "Grayscale transparent metasurface holograms," Optica **3**, 1504–1505 (2016).
23. P. Genevet, F. Capasso, F. Aieta, M. Khorasaninejad, and R. Devlin, "Recent advances in planar optics: from plasmonic to dielectric metasurfaces," Optica **4**, 139–152 (2017).
24. F. Aieta, M. A. Kats, P. Genevet, and F. Capasso, "Multiwavelength achromatic metasurfaces by dispersive phase compensation," Science **347**, 1342–1345 (2015).
25. M. Khorasaninejad, A. Ambrosio, P. Kanhaiya, and F. Capasso, "Broadband and chiral binary dielectric meta-holograms," Science Advances **2**, e1501258 (2016).
26. M. Khorasaninejad, F. Aieta, P. Kanhaiya, M. A. Kats, P. Genevet, D. Rousso, and F. Capasso, "Achromatic metasurface lens at telecommunication wavelengths," Nano Lett. **15**, 5358–5362 (2015).
27. E. Arbabi, A. Arbabi, S. M. Kamali, Y. Horie, and A. Faraon, "Multiwavelength polarization-insensitive lenses based on dielectric metasurfaces with metamolecules," Optica **3**, 628 (2016).
28. M. Khorasaninejad, W. T. Chen, R. C. Devlin, J. Oh, A. Y. Zhu, and F. Capasso, "Metalenses at visible wavelengths: Diffraction-limited focusing and subwavelength resolution imaging," Science **352**, 1190–1194 (2016).
29. S. W. Hell, S. Lindek, C. Cremer, and E. H. K. Stelzer, "Measurement of the 4pi-confocal point spread function proves 75 nm axial resolution," Appl. Phys. Lett. **64**, 1335–1337 (1994).

Optics EXPRESS

30. J. C. Miñano, P. Benitez, D. Grabovičkić, P. Zamora, M. Buljan, and B. Narasimhan, "Time multiplexing for increased FOV and resolution in virtual reality," Proc. SPIE **10335**, 1033504 (2017).
31. J. Lemos and E. Eggenberger, "Clinical utility and assessment of cyclodeviation," Current Opinion in Ophthalmology **24**, 558–565 (2013).
32. J. Courtial, T. Tyc, S. Oxburgh, J. Bělín, E. N. Cowie, and C. D. White, "Mathematica notebooks with detailed loop-imaging-theorem calculations," figshare, https://dx.doi.org/10.6084/m9.figshare.4269701.v1 (2016).